LA-UR- 08-6758

Approved for public release; distribution is unlimited.

Title:	CGMD Simulation of Interaction Between Hemagglutinin Fusion Peptides and Lipid Bilayer Membranes
Author(s):	Naveen K. Vaidya, Los Alamos National Laboratory Huaxiong Huang, York University Shu Takagi, University of Tokyo
Intended for:	Biophysical Journal

Los Alamos
NATIONAL LABORATORY
EST. 1943

Form 836 (7/06)

CGMD Simulation of Interaction between Hemagglutinin Fusion Peptides and Lipid Bilayer Membranes

Naveen K. Vaidya[1]
Department of Mathematics and Statistics,
York University, Toronto, Canada;
Currently at: Theoretical Biology and Biophysics Group,
Los Alamos National Laboratory,
Los Alamos, NM, USA

Huaxiong Huang
Department of Mathematics and Statistics,
York University, Toronto, Canada

Shu Takagi
Organ and Body Scale Team,
Computational Science Research Program, RIKEN;
Also at: Department of Mechanical Engineering,
The University of Tokyo, Tokyo, Japan

[1]Corresponding author. Address: Theoretical Biology and Biophysics Group, MS-K710, Los Alamos National Laboratory, Los Alamos, NM 87545, USA
Tel.: (505)665-6240, Fax: (505)665-3493

Abstract

Microscopic level interaction between fusion-peptides and lipid bilayer membranes plays a crucial role in membrane fusion, a key step of viral infection. In this paper, we use coarse-grained molecular dynamics (CGMD) simulations to study the interaction between hemagglutinin fusion-peptides and phospholipid bilayer membranes. With CGMD, we are able to simulate the interaction of fusion peptides with a relatively large piece of membrane for a sufficiently long time period, which is necessary for a detailed understanding of the fusion process. A conformation of the peptide with a kink at the level of phosphate group is obtained, consistent with NMR and EPR studies. Our results show that the N-terminal segment of the peptide inserts more deeply into the membrane bilayer compared to the C-terminal segment, as observed in previous experiments. Our simulations also show that the presence of fusion peptides inside the membrane may cause bilayer thinning and lipid molecule disorder. Finally, our results reveal that peptides tend to aggregate, indicating cluster formation as seen in many experiments.

Key words: Coarse-Grained Molecular Dynamics; Fusion peptide; Hemagglutinin Protein; Phospholipid bilayer; Membrane Fusion

Introduction

Membrane fusion is one of the fundamental multi-cellular biological processes, including fertilization, viral entry, release of hormones and rapid communication between neurons via neurotransmitter release and signaling (1–4). Fusion of viral enveloped and cellular membranes, which allows the delivery of viral RNAs/DNAs into a host cell, is a crucial step for any successful viral infections and virus replications. While protein-mediated membrane fusion has been studied in some detail, the mechanism is not yet well understood. Improving our knowledge of membrane fusion may help scientists to find appropriate conditions for preventing viruses such as influenza, HIV, hepatitis from fusing to and thereby infecting human cells. Understanding the virus-cell membrane fusion may also provide a clue for designing new drug delivery methods.

Viral glycoproteins, such as hemagglutinin (HA) of influenza virus and gp41 of HIV1, have been identified experimentally as mediators for the fusion process related to viral infections (5–7). As one of the best-studied fusion mediating proteins, HA consists of a trimer of individual monomers with HA1 and HA2 subunits, responsible for binding to the host cell membrane and inducing fusion, respectively. After binding, the virus internalizes into endosomes, where a low-pH (between pH 5 and 6) environment activates conformational rearrangements of the HA. During the conformational change, it reconfigures loops into helices. The subsequent translation and reorientation of the helix cause an elongation of the trimeric coiled-coil of the HA2, and the fusion peptide (consisting the first 20 amino acids of the HA2 N-terminal region) binds and inserts into a target cell membrane (8–10). Only the fusion peptide, which is a highly conserved 20 amino acid sequence present in the HA protein (6, 11–15) enters and interacts with the target membrane. Understanding this interaction is essential for a detailed understanding of the fusion mechanism.

There exist a large number of experimental studies on the fusion process and related conformational changes of HA protein and the structure of fusion peptides (12, 16–28). However, very few mathematical and computational studies (29, 30) on peptide-membrane interaction have been carried out. Experimental measurements using electron paramagnetic resonance (EPR) and nuclear magnetic resonance (NMR) have provided the structure of the HA fusion peptide inside bilayer membranes (12, 22, 24). Due to limitations of their resolution, it is difficult to use these approaches to study the effect of

the embedded peptide on bilayer integrity. As an alternative, full atomistic level molecular dynamics (MD) simulations have been carried out to determine the structure and the orientation of a HA fusion peptide inside a bilayer membrane (29, 30). However, MD is computationally intensive and existing simulation studies have been limited to a small portion of the bilayer (128 lipid molecules) with one peptide and short time duration (5-20 ns). On the other hand, it was shown that only a concerted effort of at least three to four HA-molecules (i.e., 9 to 12 fusion peptides) for a time period longer than 30 ns can lead to a successful fusion event (18). Therefore, it is necessary to develop a more efficient method, which can simulate bigger sized bilayer with many peptides for a sufficiently large time period.

In this paper, we use a coarse-grained molecular dynamics (CGMD) simulation method to study the interaction between HA fusion peptides and dipalmitoylphosphatidylcoline (DPPC) lipid bilayer membrane. CGMD allows us to perform simulations of the interaction between embedded fusion peptides and a relatively large piece of the membrane for a sufficiently long time period. The predicted structure of the peptide and the depth of the peptide residues in the bilayer system by our method are consistent with the experimental NMR and EPR results. We have also studied the effects of peptide-membrane interaction on properties such as helix tilt angle, membrane thickness, order-parameters, interaction between peptides, which are relevant for the fusion between virus and cell membranes.

Method

CG model

We consider a wild type fusion peptide of 20 amino acids "GLFGAIAGFIENGWEGMIDG", which was found experimentally to induce complete fusion. Initial coordinates of the fusion peptide are obtained from the protein data bank (PDB), where we chose a fusion peptide corresponding to a pH 5.0 environment (1IBN file) (12) (See Fig. 1).

CG-models of the phospholipid DPPC and the fusion peptide are obtained by using three-to-one, four-to-one or five-to-one mappings, i.e., three, four or five atoms are represented by a single CG particle, as suggested by Marrink et al. (31). Because of their small size and mass, hydrogen atoms are not included. A DPPC molecule is modeled using 12 CG-particles

with two tails, each of which contains four apolar particles representing 15 methyl/methylene groups as shown in Fig. 2. The head group consists of two non-polar particles representing the glycerol ester linkage (GLYC), a negatively charged particle representing the phosphate group (PO4) and a positively charged particle representing the choline moiety (NC3). Choline group and phosphate group are hydrophilic in nature while two glycerol groups are partially hydrophilic. Eight CG-particles in two tails are modeled as hydrophobic particles.

Similarly, this mapping procedure produces a CG-model of 35 CG-particles, of three different types, representing a 20 amino acids fusion peptide. Schematic diagram of the peptide CG-model is shown in Fig. 3. Each of Gly-1, Gly-4, Ala-5, Ala-7, Gly-8, Gly-13, Gly-16, Gly-20 is represented by a single CG-particle while each of Liu-2, Ile-6, Ile-10, Glu-11, Asn-12, Glu-15, Met-17, Ile-18, Asp-19 is represented by two CG-particles and each of Phe-3, Phe-9, Trp-14 is represented by three CG-particles. Based on the hydrophobicity of the residues, we have categorized into three different types: polar (Glu-11, Asn-12, Glu-15, Asp-19), non-polar (Gly-1, Gly-4, Ala-5, Ala-7, Gly-8, Gly-13, Trp-14, Gly-16, Met-17, Gly-20) and apolar (Liu-2, Phe-3, Ile-6, Phe-9, Ile-10, Ile-18). In this way, we obtain a peptide CG-model of 35 particles, in which eight particles are polar, thirteen particles are non-polar and fourteen particles are apolar. Here, polar, non-polar and apolar are hydrophilic, partial hydrophilic and hydrophobic, respectively.

The solvent is modeled by polar CG-particles, each of which represents four real water molecules. Realistic masses can be assigned to the particles, but for simplicity and for computational efficiency, we use the same masses for all particles. In particular, we use a mass of $m = 72$ amu (corresponding to four water molecules) for all CG-particles.

Interactions

All particles except the nearest neighbors interact with each other through a Lennard-Jones potential with a cutoff radius of 12 Å. The level of interaction varies according to the type of particles (polar, non-polar, apolar, charged). Nearest neighbors are connected by a weak harmonic spring. The next nearest neighbors in a DPPC interact through a harmonic angle potential and the charged groups also interact through a short-range electrostatic potential.

Nonbonded interactions

The nonbonded interactions between i^{th} and j^{th} CG-particles are described by the following Lennard-Jones (LJ) potential:

$$U_{LJ}(r) = 4\epsilon_{ij}\left[\left(\frac{\sigma_{ij}}{r}\right)^{12} - \left(\frac{\sigma_{ij}}{r}\right)^{6}\right], \tag{1}$$

where σ_{ij} and ϵ_{ij} represent the effective minimum distance of approach between two particles and the strength of their interaction, respectively. r is the distance between the centre of mass of i^{th} and j^{th} particles. According to the type of particles (polar, non-polar, apolar, charged), the level of interaction (i.e., the value of ϵ) varies among attractive (I, ϵ = 5 kJ/mol), semiattractive (II, ϵ = 4.2 kJ/mol), intermediate (III, ϵ = 3.4 kJ/mol), semirepulsive (IV, ϵ = 2.6 kJ/mol), and repulsive (V, ϵ = 1.8 kJ/mol), as suggested by Marrink et al. (31), Marrink and Mark (32). The strength of the interaction among particles is summarized in Table 1. Here, levels I, III and V interactions model strong polar interactions (bulk water), non-polar interactions in aliphatic chains and hydrophobic repulsion, respectively. Levels II and IV are of intermediate strength. We use the effective size σ_{ij} = 0.47 nm for all interaction types and the cutoff radius r_{cut} = 1.2 nm ($\approx 2.5\sigma$) for the LJ interaction potential. The cutoff noise is reduced by smoothly shifting the LJ potential to zero between a distance r_{shift} = 0.9 nm and r_{cut}. With a standard Gromacs shift function both the energy and force vanish at the cutoff distance.

In addition to LJ interaction, charged CG-particles also interact via electrostatic Coulombic potential

$$U_{el}(r) = \frac{q_i q_j}{4\pi\epsilon_0\epsilon_r r}. \tag{2}$$

Here, q_i, q_j are particle charges, ϵ_r = 20 is the relative dielectric constant. Similar to LJ potential, the electrostatic potential has a cutoff distance r_{cut} = 1.2 nm with smooth shifting from r_{shift} = 0.9 nm to r_{cut}.

Bonded interactions

Nearest neighbors are connected with a weak harmonic spring, and their bonded interaction potential is given by

$$V_{\text{bond}}(r) = \frac{1}{2}K_{\text{bond}}(r - r_0)^2, \tag{3}$$

where $r_0 = \sigma = 0.47$ nm is the equilibrium distance and $K_{\text{bond}} = 1250$ kJ mol^{-1} nm^{-2} is the force constant of the harmonic bonding potential. This force constant allows considerable deviations from the equilibrium bond length ($\sim$15%) at the cost of one kT, where k and T are Boltzmann constant and absolute temperature, respectively. The LJ interaction is excluded between bonded particles. For the angles between the next nearest particles, we use a weak harmonic potential $V_{\text{angle}}(\theta)$ of the cosine type:

$$V_{\text{angle}}(\theta) = \frac{1}{2}K_{\text{angle}}(\cos\theta - \cos\theta_0)^2, \tag{4}$$

where θ_0 is the equilibrium bond angle and $K_{\text{angle}} = 25$ kJ mol^{-1} rad^{-2} is the force constant. This force constant allows an angle deviation of 30^o at the cost of one kT. For the lipid tails (triplets GLYC-C1-C2 and PO4-GLYC-C1), an equilibrium angle of 180^o is used while an equilibrium angle of 120^o is used to model the glycerol backbone PO4-GLYC-GLYC. The LJ interaction between second nearest neighbors are not excluded. No angle potential has been used in the peptide model.

CGMD simulation

We have carried out simulations with one peptide and three peptides embedded in a piece of lipid bilayer membrane. We use a separate programme for the initialization of the system so that the minimum distance between each two particles is not less than 4 Å. For the one-peptide case, initially, a fusion peptide is placed in the upper monolayer region of the bilayer, where 122 lipids in the upper layer and 128 lipids in the lower layer are placed randomly. Similarly, for the three-peptide case, three peptides are first placed in random locations of the upper monolayer region and then 238 lipids in the upper layer and 256 lipids in the lower layer are randomly placed. Six lipids (one-peptide case) and eighteen lipids (three-peptide case) in the upper layer have been removed to make room for the fusion peptides.

As suggested in Marrink et al. (31), we use 50 water molecules per lipid (for a fully hydrated bilayer). This requires 3200 CG water particles for the one-peptide case and 6400 CG water particles for the three-peptide case, with each particle representing four water molecules. It results in 6235 CG particles for the one-peptide case and 12433 CG-particles for the three-peptide case. Based on the experimental observations that the equilibrium area per lipid for DPPC at 323 K is 0.64 nm^2 (33), the dimension of the computational unit is 90.5 Å × 90.5 Å × 200.0 Å (one-peptide case) or 128.0 Å × 128.0 Å × 200.0 Å (three-peptide case).

The simulation is performed at the temperature of 323 K. The Newton's equations of motion are integrated using the leapfrog Verlet algorithm. To ensure stability, we used an integration time step of $dt = 10$ fs. The neighbor list (non-bonded list) is updated every 10 steps using a 1.2 nm neighbor list cutoff. The pressure is maintained at 1 bar by changing the computational unit length in the z-direction (i.e. normal to the bilayer surface) while no surface tension is imposed.

We perform NVE (constant number of particles, volume and energy) simulation for 2 ns (relaxation time) before the real system starts to evolve. During early NVE simulations, we observe a significant change in the peptide conformation and it decreases slowly in later NVE simulations. Using the final configuration of NVE simulation at the end of the 2 ns period as an initial condition, we perform NPT (constant number of particles, pressure and temperature) simulations for 50 ns. Since the average properties after 30 ns do not change significantly, the results presented in this paper were calculated based on the CGMD trajectories from 20 to 30 ns. The data of every 2 ps were saved for analysis.

Tilt angle calculation

The residues 3-11 of the fusion peptide have been known to maintain a helical structure. Therefore, to analyze the tilting of the fusion peptide within the membrane, we consider these residues of the fusion peptide. Since our approach is a coarse-grained one, unlike in atomistic MD simulation, we cannot obtain a detailed helical structure of the peptide. To obtain the first order approximation of tilting, we assume that the helix-axis is a straight-line. If $\vec{A} = (x_a, y_a, z_a)$ and $\vec{B} = (x_b, y_b, z_b)$ are two points on the helix-axis, the distance from the n^{th} residue $\vec{N} = (x_n, y_n, z_n)$ to the helix-axis is given

by

$$\begin{aligned} d_n^2 &= |\vec{A}-\vec{N}|^2 - \frac{[(\vec{A}-\vec{N})\cdot(\vec{B}-\vec{A})]^2}{|\vec{B}-\vec{A}|^2} \\ &= [(x_a-x_n)^2+(y_a-y_n)^2+(z_a-z_n)^2] \\ &\quad \frac{[(x_a-x_n)(x_b-x_a)+(y_a-y_n)(y_b-y_a)+(z_a-z_n)(z_b-z_a)]^2}{(x_b-x_a)^2+(y_b-y_a)^2+(z_b-z_a)^2}. \end{aligned}$$

To find the axis, we solve the following optimization problem

$$\min_{\vec{A},\vec{B}} \sum_{n=3}^{n=11} d_n^2.$$

Let $\vec{A^m} = (x_a^m, y_a^m, z_a^m)$, $\vec{B^m} = (x_b^m, y_b^m, z_b^m)$ denote the optimal solution, the tilt angle ϕ, which is formed by the helix-axis with the normal to the bilayer surface, is given by

$$\cos\phi = \frac{z_b^m - z_a^m}{\sqrt{(x_b^m-x_a^m)^2+(y_b^m-y_a^m)^2+(z_b^m-z_a^m)^2}}.$$

Order parameter calculation

To quantify the effect of embedded peptides on the lipid bilayer, one can use the degree of order/disorder of the lipid chains in the presence of peptides. For this purpose, we have calculated the second-rank order parameter for consecutive bonds using the following formula:

$$S = \left\langle \frac{1}{2}(3\cos^2\theta - 1) \right\rangle,$$

with

$$\cos\theta = \frac{r_z^j - r_z^i}{\sqrt{(r_x^j-r_x^i)^2+(r_y^j-r_y^i)^2+(r_z^j-r_z^i)^2}},$$

where θ is the angle between the bilayer normal and the bond joining two consecutive lipid CG particles $\vec{r^i} = (r_x^i, r_y^i, r_z^i)$ and $\vec{r^j} = (r_x^j, r_y^j, r_z^j)$. $S = 1$ indicates the perfect alignment with the bilayer normal, while $S = -0.5$ corresponds to alignment parallel to bilayer surface and $S = 0$ indicates a

random orientation. $\langle\rangle$ represents the average over all the lipids in upper layer or in lower layer of the lipid bilayer.

Results and Discussion

Since the simulation time required for a given system to reach an equilibrium state depends on the choice of initial peptide configuration, in general it may be necessary to choose random initial configurations to minimize computational bias. However, the objective of this study is not to observe the folding/refolding mechanism. Therefore, it is not necessary to start with a random configuration. The initial configuration of the peptide we have taken is the bilayer-bound conformation of the fusion peptide obtained by NMR at pH 5.0 (12) [PDB code: 1IBN]. Thus, our results can be treated as simulations of a real experimental system.

Structure of the bilayer bound peptide

Snapshots of a simulation at t = 0, 6, 12, 18, 24, 30 ns are shown in Fig. 4. Some CG particles of lipid and water have been removed for clarity. They show that the overall structure of the fusion peptide inside the membrane takes an angled V-shape with most of the bulky apolar residues pointing towards a hydrophobic pocket in the center of the V shape. This structure is similar to those obtained by NMR and EPR (12, 34) as well as on atomistic simulations (MD simulations) (29, 30). Our simulation shows that there is always a kink near the Asn-12 residue which agrees with experimental observations. It has been pointed out that this is an extremely important structure for a successful fusion to occur (23, 34). We also found that the angle of the V-shape peptide at the location of the kink may vary considerably during simulations.

The most stable three-dimensional structure of the peptide inside the membrane is shown in Fig. 5, where lipid and water particles are again removed for clarity. CG particles containing α-carbon of the 20 amino acids are marked by 1,2,...,20. Note that the membrane surface is parallel to the XY-plane. This structure shows that the polar particles (green) Glu-11, Asn-12, Glu-15, Asp-19 try to stay close the surface of the membrane and the apolar particles (red) Leu-2, Phe-3, Ile-6, Phe-9, Ile-10, Ile-18 have the tendency to immerse deep into the membrane while the partially hydrophilic non-polar

particles remain somewhere in between. Such characteristics of the particles cause the peptide structure to form a V–shape with a kink near Asn-12. The relative position of each particle agrees well with the NMR data in Han et al. (12) (c.f. Fig. 1). The angled V-shape structure with a kink around Asn-12 residue appears also in simulations of a larger domain containing three peptides. In the three-peptide case, the angle at the kink is not necessarily the same for all peptides.

NMR data on the fusion peptide shown in Han et al. (12) indicate that residues 3-11 form an α-helix. The coarse-grained approach used in our study does not provide a detailed secondary structure of the peptide. Nonetheless, we can compute the distance between the CG-particles containing carbonyl (C=O) group of i^{th} amino acid and the CG-particles containing amino (N-H) group of $(i+4)^{th}$ amino acid. Even though this distance does not represent the true hydrogen bonding, it provides some information of α-helix structure. The time evolution of the distance between Phe-3 and Ala-7, Gly-4 and Gly-8, Ala-5 and Phe-9, Ile-6 and Ile-10, Ala-7 and Glu-11 is shown in Fig. 6. The last graph in Fig. 6 shows the time evolution of the maximum and minimum of these distances. Horizontal lines in the figure represent the mean value. The average distances between Phe-3 and Ala-7, Gly-4 and Gly-8, Ala-5 and Phe-9, Ile-6 and Ile-10, Ala-7 and Glu-11 are 7.5, 6.6, 6.8, 8.0, 7.0 Å, respectively. Moreover, the distance remains between the minimum average 4.8 Å and the maximum average 9.6 Å (last graph). These numbers are reasonably close to a rise per helix-turn of 5.4 Å. Therefore, an α-helix structure formed by residues 3-11 of the fusion peptide is indicated inside the lipid bilayer membrane, in agreement with the NMR study (12).

We note that due to the coarse-grained approach used in this sudy, we are unable to further discuss the atomistic detail of the peptide structure. However, many important average properties relevant to the fusion process can be obtained and are discussed below.

Position and orientation of peptide

Fig. 7(a) shows the distance from the residues to the average phosphate group obtained by NMR (12) and our simulations (averaged over the CGMD trajectories from 20 to 30 ns). We can clearly see a kink structure near the Asn-12 residue at the same position of the phosphate group of the lipid bilayer, consistent with experimental observations (12). The peptide penetrates the bilayer with a distance about 10 Å, which is slightly less than the NMR

value. Among all the residues, Leu-2 and Phe-3 are the ones most deeply inserted into the bilayer. For simulations with multiple peptides shown in Fig. 7(b), the penetration distance varies. Some peptides can penetrate deeper than the others, all the way to the lower mono layer. Contrary to the singe peptide case, Gly-4 and Ala-5 of some peptides of the three peptide case are the most deeply inserted amino acids (See Peptide-II in Fig. 7(b)). Residues Trp-14, Gly-16, Asp-19 are at the same position of the phosphate group. Asn-12 and Glu-15 are mostly projected into the bulk water.

Our simulation shows that hydrophobic residues including Leu-2, Phe-3, Ile-6, Phe-9, Ile-10 and Ile-18 form hydrophobic pockets pointing towards the central plane of the bilayer. On the other hand, hydrophilic residues Glu-11, Asn-12, Glu-15 and Asp-19 are oriented towards the lipid head group. Such an arrangement of hydrophilic and hydrophobic residue groups was found to be important for fusion activity (29). Furthermore, the N-terminal segment Gly-1 to Ile-10 inserts more deeply into the membrane bilayer, compared to the C-terminal segment Glu-11 to Gly-20. As seen in the three-peptide case (Fig. 7(b)), a penetration due to N-terminal segment (Gly-1 to Ile-10) may vary from peptide to peptide while a penetration due to C-terminal segment (Glu-11 to Gly-20) remains the same for all the peptides. A slight discrimination in the penetration of C-terminal segment between the experimental and the simulation results in Fig. 7(a) might be due to the fact that the C-terminus is positioned inside the membrane in the experimental setting while we allowed the C-terminal to move freely in our simulation.

Since the kink near the Asn-12 residue is important for fusion, we have presented its position measured from the average phosphate group from 20 ns to 30 ns in Fig. 8, for the one-peptide and three-peptide cases. The Asn-12 residue fluctuates at the level of the phosphate group. It can move deeply into the bilayer (up to 10 Å) in one-peptide case and to 15 Å for some peptide in three-peptide case, especially in the beginning, and come out of the surface (up to 5 Å). On average, it remains on the surface side but stays close to the phosphate group. Therefore, the results show that the kink as well as the peptide can penetrate into the lipid bilayer.

We have shown earlier that the fusion peptide maintains its helical structure from Phe-3 to Glu-11. The orientation of the peptide can be measured by the tilt angle between the helix-axis and the plane of the membrane. The time evolution of the tilt angle for one-peptide case from 20 ns to 30 ns is shown in Fig. 9(a). A thick horizontal line in the figure indicates the average tilt angle and two dotted lines are the standard deviation. The helix-axis is

found to be tilted with an orientation of $\sim 30 \pm 15^o$. The average orientation of $\sim 30^o$ is in fairly good agreement with experimental results of $\sim 25^o$ obtained by mapping NMR data onto the best fit EPR data (12) and $\sim 38^o$ obtained from EPR data on singly spin-labeled peptides (23, 24). The fluctuation around the average tilt angle is quit large in our simulation compared to the experimental observation. To show the effect of multiple peptides on the tilt angle, the helix tilt-angle for each peptide is shown in Fig. 9(b). The average angle is shown by horizontal lines. For clarity, lines of the standard deviation have been omitted in Fig. 9(b). It can be seen that the helical-axis orientation is not consistent for all peptides. The helix-axis orientation is $\sim 32 \pm 13^o$, $\sim 58 \pm 13^o$ and $\sim 45 \pm 13^o$, for peptide-I, peptide-II and peptide-III, respectively. Fluctuation around the average tilt angle of helix axis is slightly less in three-peptide case compared to the one-peptide case. Penetration as well as orientation of peptides can vary widely in the three-peptide case.

Interaction between peptides

It has been experimentally observed that HA-mediated fusion requires a concerted and cooperative action of at least three to four HA trimers (18). An early stage of the fusion process involves cluster formation of at least three to four trimers, i.e., a cluster of at least nine to twelve fusion peptides. Therefore, interaction among the fusion peptides is important for a successful fusion event. Since the three fusion peptides of our simulated system have been placed randomly inside the lipid bilayer membrane, these fusion peptides could represent fusion peptides of the same or different HA molecules. In order to show the tendency of fusion peptides to aggregate, we have plotted the time-evolution from 20 ns to 30 ns of the distances between the center of mass of each two peptides (peptides I and II, II and III, III and I) in Fig. 10. Our simulation shows that there is a sufficient lateral mobility of the fusion peptides inside the lipid bilayer similar to what is observed in the experiment by Danieli et al. (18). From 20 to 30 ns, the distance between peptides I and II, II and III, III and I, decreases from ~ 100 Å to ~ 60 Å, ~ 60 Å to ~ 50 Å and ~ 40 Å to ~ 15 Å, respectively. It clearly shows that the fusion peptides have a tendency to aggregate, indicating the formation of clusters.

Effect of peptides on the lipid bilayer

Experimental evidences revealed that the insertion of the HA fusion peptide affects the organization of the bilayer (35–38). In this study, we examine two characteristics of the bilayer, namely bilayer thickness (between upper and lower phosphate groups) and a second-rank order parameter. We note that only three fusion peptides are used in our simulation which is less than the required 9-12 fusion peptides for a successful fusion activity.

Fig. 11 shows the time evolution of the bilayer thickness measured between (averaged) phosphate groups of upper and lower layers for both one-peptide and three-peptide cases. The average bilayer thickness in the one-peptide case is $\sim$41.1$\pm$0.4 Å, which is slightly larger than the value (without peptide) obtained by previous CG simulation (40$\pm$1 Å) (31) and experimental measurements (38.5 Å) (33). In the three-peptide case, the bilayer thickness is $\sim$38.9$\pm$0.3 Å. The bilayer thickness change is a combined result of vertical fluctuation and tilting of lipid molecules. Both the average bilayer thickness and the fluctuation around the average thickness in the three-peptide case are less than that in the one-peptide case. Therefore, one can conclude that an increase in the number of peptides enhances the bilayer thinning, which is required for the formation of a pore in the fusion. Moreover, an increase in the number of embedded peptides also reduces the thickness fluctuation around the average value. This might be due to the fact that a presence of peptides imposes a constraint on the lipid molecules. Our simulation also shows that using one peptide or three peptides is not sufficient to reduce the bilayer thickness significantly, supporting experimentally observed fact that the fusion process is mediated by a concerted activity of many proteins (18).

For a further detailed understanding of the lipid conformation and the lipid packing, we have calculated the second-rank order parameter $S = \langle 0.5(3\cos^2\theta - 1)\rangle$ for consecutive bonds, where θ is the angle formed by the bond with the bilayer normal (See Method Section). The order parameter for upper layer and lower layer is shown in Fig. 12. The figure includes the order parameter in the presence of both one and three peptides. As in the case of the bilayer without peptide (31, 32), both the phosphate-choline bond and the glycerol linkage have a predominantly parallel orientation with respect to the surface normal, whereas the other bonds' orientation is along the surface normal. The value decreases towards the end of the tail. Effect of peptides on the order parameter occurs near the hydrocarbon chain while the order

parameter towards the head group remains almost the same. An increase in the number of peptides decreases the value of the order parameter, suggesting that the lipids are more disordered due to the presence of peptides. To a less degree, this effect can also be seen in the lower lipid monolayer. A decrease in order parameter of hydrocarbon chain indicates that the peptides enhance the tilting of the hydrocarbon chain. A smaller order parameter in the presence of three peptides is in accordance with the bilayer thinning as we explained earlier. Once again, we would like to note that the decrease in order parameter reported in this paper is not sufficient for fusion to take place since only three fusion peptides are used in the simulations.

Conclusion

We have presented the results of the interaction between the influenza HA fusion peptides and a phospholipid DPPC bilayer membrane by using coarse-grained molecular dynamics (CGMD) simulations. CGMD simulations can be carried out for a system consisting of a relatively large piece of lipid membrane and many peptides for a relatively long physical time period, which is necessary for a detailed understanding of the fusion process. The CGMD method is computationally efficient in terms of system size and runtime, compared to the atomistic MD simulation. Our simulation produced a V-shaped conformation of the fusion peptide with a kink at Asn-12 residue, consistent with NMR and EPR studies (12). The averaged position of the kink remains near the phosphate group. Our simulation also predicted the correct arrangement of hydrophobic and hydrophilic residues, which is important for fusion activity.

Helical structure of the peptide from residues 3-11 is indicated by our simulation, consistent to the experiments (12) and the orientation of the helix-axis varies from peptide to peptide. Our results show that the insertion of the N-terminal segment of the peptide into the membrane is deeper than the C-terminal segment. Moreover, the depth of insertion of the N-terminal segment varies among peptides while that of C-terminal segment remains the same for all peptides. Our simulation also reveals that peptides tend to aggregate, which is a good indication of the formation of clusters for performing concerted action required for fusion.

Our results show that an increase in the number of embedded fusion peptides causes lipid molecules disorder and reduces bilayer thickness, but the

thinning due to one or three peptides is not sufficient for fusion. This supports the experimental observation that fusion is possible only by a concerted effort of many protein molecules. Therefore, to mimic a more realistic fusion process in the CGMD model, one of the possible future extensions of this work is to use a system with sufficiently many peptides. Moreover, since the viruses have a tendency to mutate, it is important to carry out simulations for the fusion peptide of other mutants as well.

Finally, it is worthwhile to note that our approaches could be applied for the study of fusion processes related to other viruses such as HIV and Hepatitis B, C. It could also be used for the study of general protein-membrane interaction, which exists in many normal physiological phenomena within living organisms.

Acknowledgement. This research was supported by the Susan Mann Dissertation Scholarship Award of York University; Natural Science and Engineering Research Council (NSERC) of Canada; Mathematics for Information Technology and Complex System (MITACS) of Canada; and Research and Development of the Next-Generation Integrated Simulation of Living Matter, a part of the Development and Use of the Next-Generation Supercomputer Project of the Ministry of Education, Culture, Sports, Science and Technology (MEXT). The first author wishes to thank The University of Tokyo for providing a visiting fellowship while part of this research was carried out and Mr. Tomofumi Osaki for his valuable help in coding and computation.

References

1. Chernomordik, L. V., and M. M. Kozlov, 2003. Protein-lipid interplay in fusion and fission of biological membranes. *Anne. Rev. Biochem.* 72:175–207.

2. Harrison, S. C., 2008. Viral membrane fusion. *Nat. Struct. Mol. Biol.* 15:690–698.

3. Karli, U. O., T. Schafer, and M. M. Burger, 1990. Fusion of neurotransmitter vesicles with target membrane is calcium independent in a cell-free system. *PNAS* 87:5912–5915.

4. Kasson, P. M., N. W. Kelley, N. Singhal, M. Vrljic, A. T. Brunger, and

V. S. Pande, 2006. Ensemble molecular dynamics yields submillisecond kinetics and intermediates of membrane fusion. *PNAS* 103:11916–11921.

5. Cross, K. J., S. A. Wharton, J. J. Skehel, D. C. Wiley, and D. A. Steinhauer, 2001. Studies on influenza hemagglutinin fusion peptide mutants generated by reverse genetics. *EMBO J.* 20:4432–4442.

6. Wilson, I. A., J. J. Skehel, and D. C. Wiley, 1981. Structure of the hemagglutinin membrane glycoprotein of influenza virus at 3 Angstrom resolution. *Nature* 289:366–373.

7. Chan, D. C., D. Fass, J. M. Berger, and P. S. Kim, 1997. Core Structure of gp41 from the HIV envelop glycoprotein. *Cell* 89:263–273.

8. Bullough, P. A., F. M. Hughson, J. J. Skehel, and D. C. Wiley, 1994. Structure of influenza hemagglutinin at the pH of membrane fusion. *Nature* 371:37–43.

9. Carr, C. M., and P. S. Kim, 1993. A spring-loaded mechanism for the conformational change of influenza hemagglutinin. *Cell* 73:823–832.

10. Skehel, J. J., and D. C. Wiley, 2000. Receptor binding and membrane fusion in virus entry: the influenza hemagglutinin. *Annu. Rev. Biochem.* 69:531–569.

11. Daniels, R. S., J. C. Downie, A. J. Hay, M. Knossow, J. J. Skehel, M. L. Wang, and D. C. Wiley, 1985. Fusion mutants of the influenza virus hemagglutinin glycoprotein. *Cell* 40:431–439.

12. Han, X., J. H. Bushweller, D. S. Cafiso, and L. Tamm, 2001. Membrane structure and fusion-triggering conformational change of the fusion domain from influenza hemagglutinin. *Nat. Struct. Biol.* 8:715–720.

13. Isin, B., P. Dokuker, and I. Bahar, 2002. Functional Motions of Influenza Virus Hemagglutinin: A Structure-Based Analytical Approach. *Biophys. J.* 82:569–581.

14. Weis, W. I., S. C. Cusack, J. H. Brown, R. S. Daniels, J. J. Skehel, and J. D. Watson, 1990. The structure of a membrane fusion mutant of the influenza virus hemagglutinin. *EMBO J.* 9:17–24.

15. White, J. M., 1992. Membrane Fusion. *Science* 258:917–924.

16. Bentz, J., H. Ellens, and D. Aalford, 1990. An architecture for the fusion site of influenza hemagglutinin. *FEBS Lett.* 276:1–5.

17. Blumenthal, R., C. C. Pak, Y. Raviv, M. Krumbiegel, L. D. Bergelson, S. J. Morris, and R. J. Lowy, 1995. Transient domains induced by influenza hemagglutinin during membrane fusion. *Mol. Membr. Biol.* 12:135–142.

18. Danieli, T., S. L. Pelletier, Y. I. Henis, and J. M. White, 1996. Membrane fusion mediated by the influenza virus hemagglutinin requires the concerted action of at least three hemaglutinin trimer. *J. Cell Biol.* 133:559–569.

19. Gaudin, Y., R. W. H. Ruigrok, and J. Brunner, 1995. Low-pH induced conformational changes in viral fusion proteins: implications for the fusion mechanism. *J. Gen. Virol.* 76:1541–1556.

20. Gruenke, J. A., R. T. Armstrong, W. W. Newcomb, J. C. Brown, and J. M. White, 2002. New insights into the spring-loaded conformational change of influenza virus hemagglutinin. *J. Virol.* 76:4456–4466.

21. Gutman, O., T. Danieli, J. M. White, and Y. I. Henis, 1993. Effects of exposure to low pH on the lateral mobility of influenza hemagglutinin expressed at the cell surface: correlation between mobility inhibition and inactivation. *Biochem.* 32:101–106.

22. Han, X., and L. K. Tamm, 2000. A host-guest system to study structure-function relationships of membrane fusion peptides. *Proc. Natl. Acad. Sci., USA* 97:13097–13102.

23. Li, Y., X. Han, A. L. Lai, J. H. Bushweller, D. S. Cafiso, and L. K. Tamm, 2005. Membrane structures of the hemifusion-inducing fusion peptide mutant G1S and the fusion-blocking mutant G1V of influenza virus hemagglutinin suggest a mechanism for pore opening in membrane fusion. *J. Virol.* 79:12065–12076.

24. Macosko, J. C., C. H. Kim, and Y. K. Shin, 1997. The membrane topology of the fusion peptide region of influenza hemagglutinin determined by spin-labeling EPR. *J. Mol. Biol.* 267:1139–1148.

25. Markovic, I., E. Leikina, M. Zhukovsky, J. Zimmerberg, and L. V. Chernomordik, 2001. Synchronized activation and refolding of influenza hemagglutinin in multimeric fusion machines. *J. Cell Biol.* 155:833–843.

26. Markosyan, R. M., G. B. Melikyan, and F. S. Cohen, 1999. Tension of membranes expressing the Hemagglutinin of influenza virus inhibits fusion. *Biophys. J.* 77:943–952.

27. Stegmann, T., 1993. Influenza hemagglutinin-mediated membrane fusion does not involve inverted phase lipid intermediates. *J. Biol. Chem.* 268:1716–1722.

28. Tamm, L. K., F. Abildgaard, A. Arora, H. Blad, and J. H. Bushweller, 2003. Structure, dynamics and function of the outer membrane protein A (OmpA) and influenza hemagglitinin fusion domain in detergent micelles by solution NMR. *FEBS Letters* 555:139–143.

29. Huang, Q., C. Chen, and A. Herrmann, 2004. Bilayer conformation of fusion peptide of influenza virus hemagglutinin: a molecular dynamics simulation study. *Biophys. J.* 87:14–22.

30. Vaccaro, L., K. L. Cross, J. Kleinjung, S. K. Straus, D. J. Thomas, S. A. Wharton, J. J. Skehel, and F. Fraternali, 2005. Plasticity of influenza hemagglutinin fusion peptides and their interaction with lipid bilayers. *Biophys. J.* 88:25–36.

31. Marrink, S. J., A. H. Vries, and A. E. Mark, 2004. Coarse Grained Model for Semiquantitative Lipid Simulations. *J. phys. Chem. B* 108:750–760.

32. Marrink, S. J., and A. E. Mark, 2003. Molecular dynamics simulation of the formation, structure, and dynamics of small phospholipid vesicles. *J. Am. Chem. Soc.* 125:15233–15242.

33. Nagle, J. F., and S. Tristram-Nagle, 2000. Structure of lipid bilayers. *Biochim. Biophys. Act* 1469:159–195.

34. Tamm, L. K., X. Han, Y. Li, and A. L. Lai, 2002. Structure and function of membrane fusion peptides. *Biopolymer (Peptide Science)* 66:249–260.

35. Colotto, A., and R. M. Epand, 1997. Structural study of the relationship between the rate of membrane fusion and the ability of the fusion peptide of influenza virus to purturb bilayer. *Biochem.* 36:7644–7651.

36. Epand, R. M., 1998. Lipid polymorphism and protein-lipid interactions. *Biochim. Biophys. Acta.* 1376:353–368.

37. Han, X., D. A. Steinhauer, S. A. Wharton, and L. K. Tamm, 1999. Interaction of mutant influenza virus hemagglutinin fusion peptides with lipid bilayers: probing the role of hydrophobic residue size in the central region of the fusion peptide. *Biochem.* 38:15052–15059.

38. Siegel, D. P., and R. M. Epand, 2000. Effect of influenza hemagglutinin fusion peptide on lamellar/inverted phase transitions in dipalmitoleoylphosphatidylethanolamine: implicatitons for membrane fusion mechanisms. *Biochim. Biophys. Act* 1468:87–98.

Table 1: Level of interaction I (attractive, $\epsilon = 5$ kJ/mol), II (semiattractive, $\epsilon = 4.2$ kJ/mol), III (intermediate, $\epsilon = 3.4$ kJ/mol), IV (semirepulsive, $\epsilon = 2.6$ kJ/mol) or V (repulsive, $\epsilon = 1.8$ kJ/mol). Five different groups considered are polar (PO), positively charged (Q+), negatively charged (Q-), non-polar (NP) and apolar (AP).

Group	PO	Q+	Q-	NP	AP
PO	I	I	I	III	V
Q+	I	III	III	III	V
Q-	I	III	III	III	V
NP	III	III	III	II	IV
AP	V	V	V	IV	III

Figure Legends

Figure 1.

NMR structure of a fusion peptide inside a detergent micelle at low pH (12) [PDB code:1IBN].

Figure 2.

CG model of a lipid molecule.

Figure 3.

CG model of a fusion peptide.

Figure 4.

Snapshots of the conformation of HA fusion peptide inside the bilayer at t = 0, 6, 12, 18, 24, 30 ns.

Figure 5.

Membrane-bound peptide structure showing CG particles containing α-carbon of 20 amino acids. For clarity, lipid and water particles have been removed.

Figure 6.

Time evolution of the distance from CG particles containing carbonyl (C=O) group of Phe-3, Gly-4, Ala-5, Ile-6, Ala-7 to CG particles containing amino (N-H) group of Ala-7, Gly-8, Phe-9, Ile-10, Glu-11, respectively. The last graph shows the maximum and minimum of these distances.

Figure 7.

Depth of insertion (distance to the lipid phosphate group) of 20 residues of HA fusion peptide at pH 5.0 for (a) one-peptide case and (b) three-peptide case. The experimental data is from Fig. 5 of citehan01.

Figure 8.

Time evolution of the distance of Asn-12 residue from the lipid phosphate group for the (a) one-peptide case, and the (b) three-peptide case.

Figure 9.

Time evolution of the orientation of the helical axis (Residue Phe-3 to Glu-11) with respect to the bilayer surface in the (a) one-peptide case, and (b) three-peptide cases.

Figure 10.

Time evolution of the distances between the center of mass of each two peptides (peptides I and II, II and III, III and I).

Figure 11.

Time evolution of the bilayer thickness measured between averaged upper and lower phosphate groups for the one-peptide and the three-peptide cases. The thick lines represent the average thickness and the broken lines indicate the standard deviation of the bilayer thickness.

Figure 12.

The second-rank order parameter of consecutive bond (in the lipid molecule) with respect to the surface normal for (a) upper lipid monolayer (b) lower lipid monolayer.

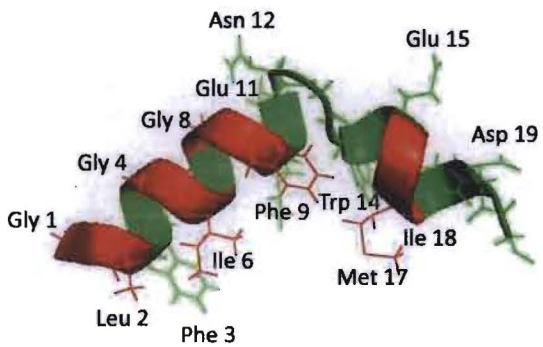
Asn 12
Glu 15
Glu 11
Gly 8
Asp 19
Gly 4
Phe 9
Trp 14
Gly 1
Ile 18
Ile 6
Met 17
Leu 2
Phe 3

Figure 1:

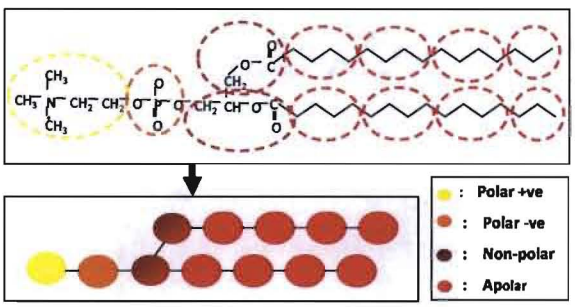

Figure 2:

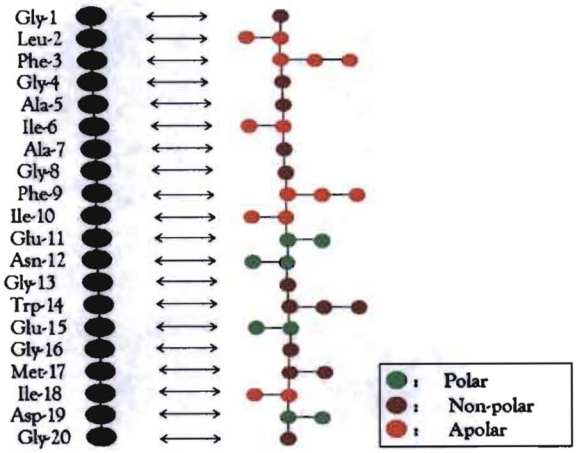
Gly-1
Leu-2
Phe-3
Gly-4
Ala-5
Ile-6
Ala-7
Gly-8
Phe-9
Ile-10
Glu-11
Asn-12
Gly-13
Trp-14
Glu-15
Gly-16
Met-17
Ile-18
Asp-19
Gly-20
Polar
Non-polar
Apolar

Figure 3:

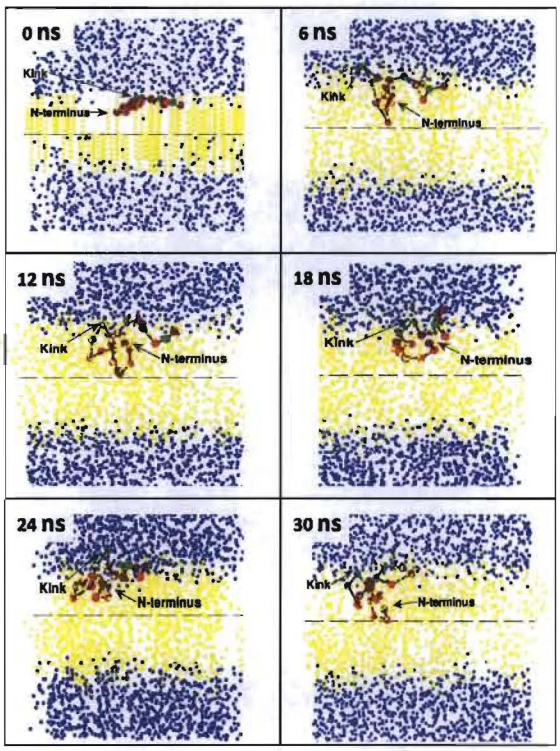
0 ns
Kink
N-terminus
6 ns
Kink
N-terminus
12 ns
Kink
N-terminus
18 ns
Kink
N-terminus
24 ns
Kink
N-terminus
30 ns
Kink
N-terminus

Figure 4:

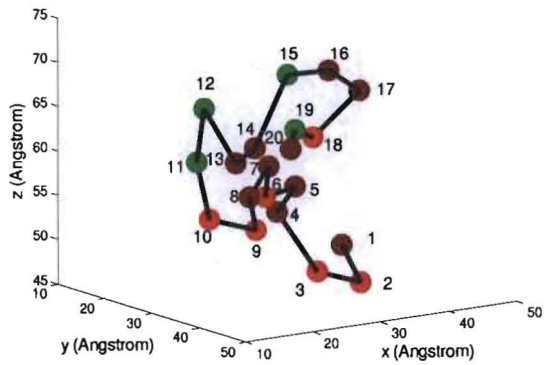
z (Angstrom)
y (Angstrom)
x (Angstrom)
1
2
3
4
5
6
7
8
9
10
11
12
13
14
15
16
17
18
19
20

Figure 5:

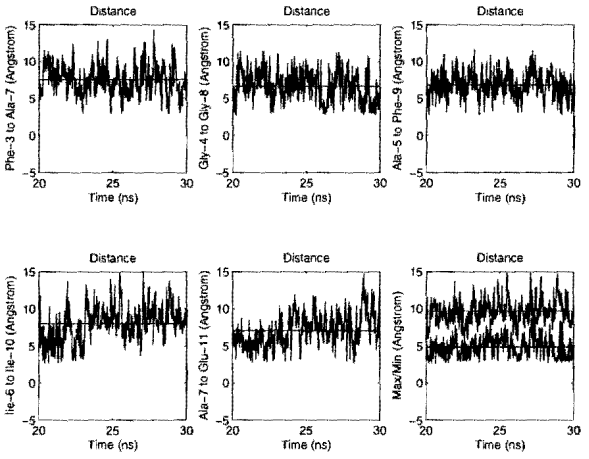
Distance
Phe-3 to Ala-7 (Angstrom)
Gly-4 to Gly-8 (Angstrom)
Ala-5 to Phe-9 (Angstrom)
Ile-6 to Ile-10 (Angstrom)
Ala-7 to Glu-11 (Angstrom)
Max/Min (Angstrom)
Time (ns)
15
10
5
0
-5
20
25
30

Figure 6:

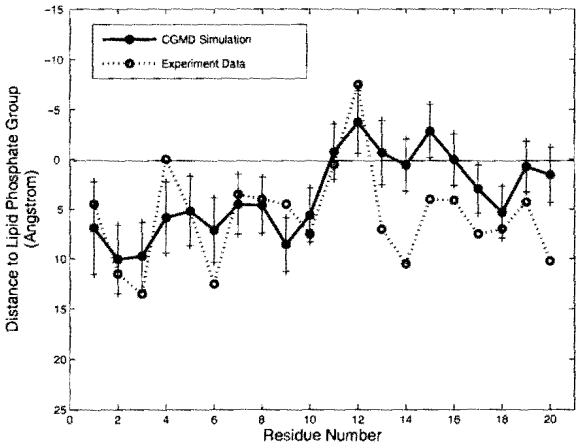
CGMD Simulation
Experiment Data
Distance to Lipid Phosphate Group (Angstrom)
Residue Number

(a)

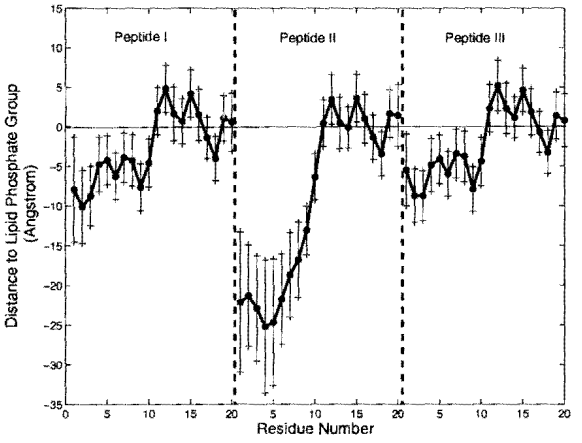
Peptide I
Peptide II
Peptide III
Distance to Lipid Phosphate Group (Angstrom)
Residue Number

(b)

Figure 7:

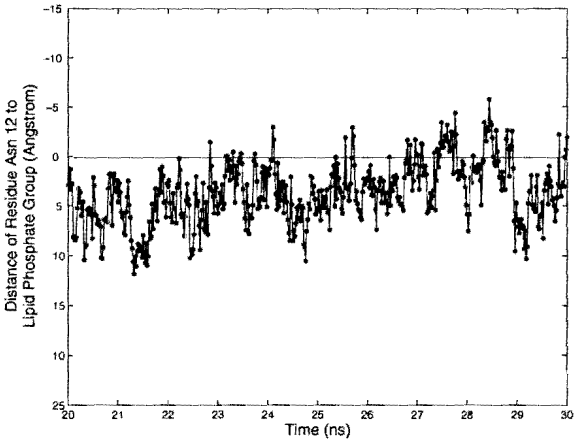
Distance of Residue Asn 12 to Lipid Phosphate Group (Angstrom)
Time (ns)

(a)

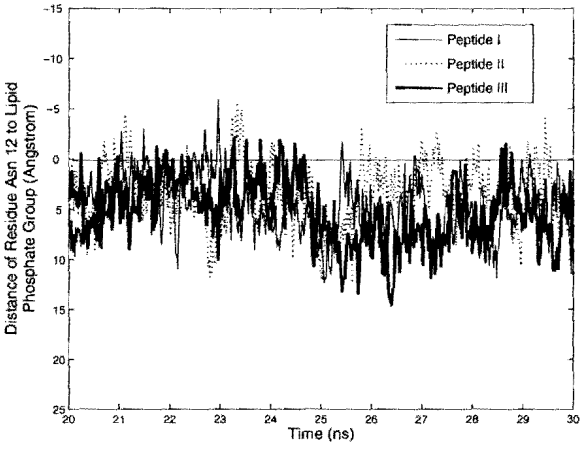
Peptide I
Peptide II
Peptide III
Distance of Residue Asn 12 to Lipid Phosphate Group (Angstrom)
Time (ns)

(b)

Figure 8:

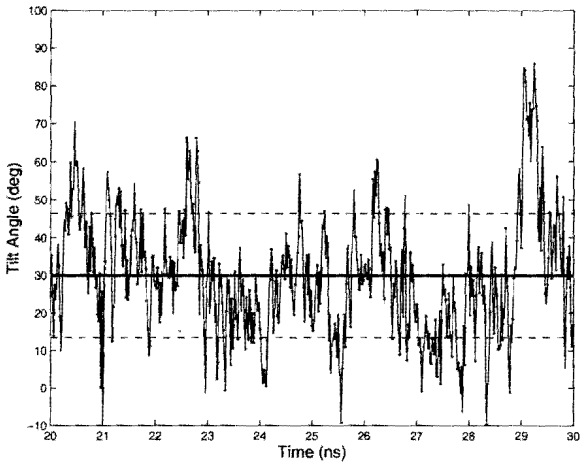
Tilt Angle (deg)
Time (ns)

(a)

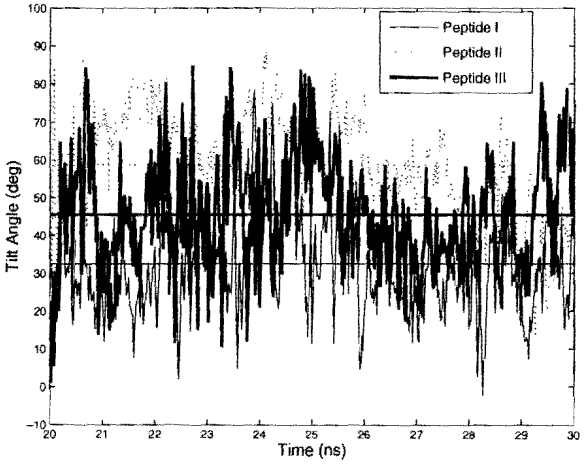
Peptide I
Peptide II
Peptide III
Tilt Angle (deg)
Time (ns)

(b)

Figure 9:

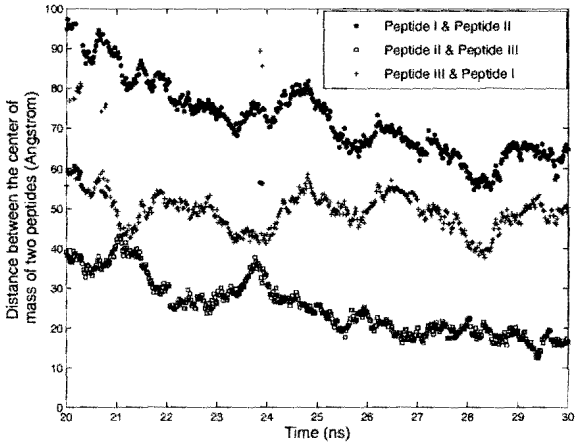
Peptide I & Peptide II
Peptide II & Peptide III
Peptide III & Peptide I
Distance between the center of mass of two peptides (Angstrom)
Time (ns)
0
10
20
30
40
50
60
70
80
90
100
20
21
22
23
24
25
26
27
28
29
30

Figure 10:

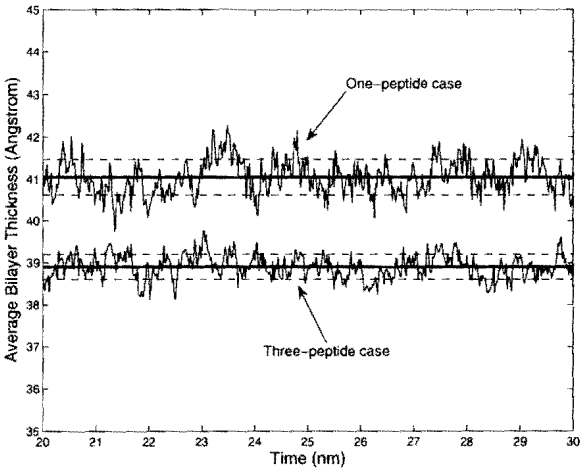
One–peptide case
Three–peptide case
Average Bilayer Thickness (Angstrom)
Time (nm)
45
44
43
42
41
40
39
38
37
36
35
20
21
22
23
24
25
26
27
28
29
30

Figure 11:

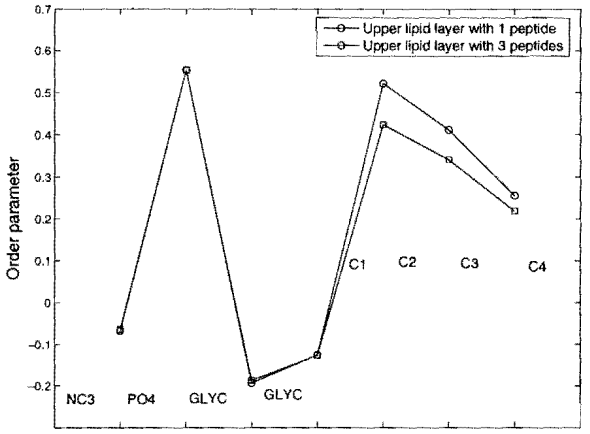
Upper lipid layer with 1 peptide
Upper lipid layer with 3 peptides
Order parameter
0.7
0.6
0.5
0.4
0.3
0.2
0.1
0
-0.1
-0.2
C1
C2
C3
C4
NC3
PO4
GLYC
GLYC

(a)

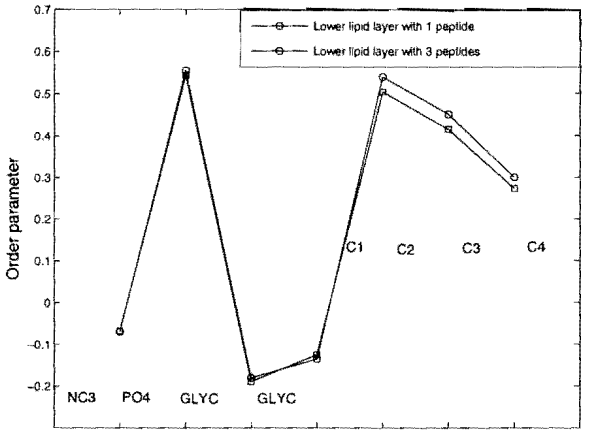
Lower lipid layer with 1 peptide
Lower lipid layer with 3 peptides
Order parameter
0.7
0.6
0.5
0.4
0.3
0.2
0.1
0
-0.1
-0.2
C1
C2
C3
C4
NC3
PO4
GLYC
GLYC

(b)

Figure 12: